Topotactic Intercalation of Water and Pyridine into Co(H2PO2)2.cntdot.nH2O (0 .ltoreq. n .ltoreq. 0.69). Crystal Structure of Co(H2PO2)2.cntdot.0.53H2O Solved from X-ray Powder Dif...

ARTICLE *in* INORGANIC CHEMISTRY · MARCH 1994

Impact Factor: 4.76 · DOI: 10.1021/ic00084a042

4 AUTHORS, INCLUDING:

Pedro Amorós
University of Valencia
220 PUBLICATIONS **4,984** CITATIONS
SEE PROFILE

Daniel Beltrán-Porter
University of Valencia
237 PUBLICATIONS **4,428** CITATIONS
SEE PROFILE

Topotactic Intercalation of Water and Pyridine into $Co(H_2PO_2)_2 \cdot nH_2O$ ($0 \leq n \leq 0.69$). Crystal Structure of $Co(H_2PO_2)_2 \cdot 0.53H_2O$ Solved from X-ray Powder Diffraction Data

M. Dolores Marcos, Pedro Amorós,* Daniel Beltrán, and Aurelio Beltrán

UIBCM, Departament de Química Inorgánica, Facultat de Quimiques, Universitat de València, Dr. Moliner No. 50, 46100-Burjassot (València), Spain

Received August 6, 1993®

The synthesis of differently hydrated layered cobalt hypophosphites, $Co(H_2PO_2)_2 \cdot nH_2O$ ($0 \leq n \leq 0.69$), has been possible by carefully controlling the water content in the reaction medium. The crystal structure of $Co(H_2PO_2)_2 \cdot 0.53H_2O$ has been refined from X-ray powder diffraction data by the Rietveld method, using as a starting model the structural parameters of the orthorhombic anhydrous zinc hypophosphite $Zn(H_2PO_2)_2$. The cell is monoclinic (space group $P112/a$; $Z = 2$) with $a = 6.4722(3)$ Å, $b = 5.3411(3)$ Å, $c = 7.4900(3)$ Å and $\gamma = 90.087(12)°$. The final reliability factors were, $R_I = 5.38\%$, $R_p = 7.31\%$, and $R_{wp} = 9.05\%$. The lamellar structure can be thought of as constructed from corrugated rutile like chains of cationic edge-sharing octahedra running along the a axis and interconnected in the b direction through hypophosphite bridges. $Co(H_2PO_2)_2 \cdot nH_2O$ compounds are suitable hosts lattices for intercalation reactions. Water and pyridine intercalation processes in these matrices have been studied by thermal analysis, variable-temperature X-ray powder diffraction, and spectroscopic techniques. A structural proposal for $Co(H_2PO_2)_2 \cdot 1.86(C_5H_5N) \cdot 0.31H_2O$ is presented.

Introduction

The intercalation of guest molecules in layered hosts has received considerable attention in recent years owing to the potential that such materials show for catalysis, molecular sieving, and ion exchange. Intercalation can be considered a reversible topotactic reaction of a solid host (H), which provides an interconnected system of accessible unoccupied lattice sites (□), with ambient mobile guest species (G) that can diffuse into the solid and occupy the empty positions according to the following reaction scheme: $xG + \square_x[H] \Leftrightarrow G_x[H]$. The term topotactic refers to the idea that the host matrix units retain their integrity with respect to the structure and composition in the course of intercalation and deintercalation. A considerable number of solids with layered structures (clays, graphite, transition metal chalcogenides, oxide bronzes, zirconium phosphates, vanadium phosphates, etc.) have proved to be suitable host for intercalation, whereas the nature of the guest species (ions or neutral molecules, metal complexes, etc.) is related to the binding modes that these entities may establish with the host lattice (ionic or covalent bonds, van der Waals interactions,..).[1-3]

Following our work on oxovanadium phosphates,[4] we explored the idea that the formation of new low dimensional systems (in particular lamellar solids able to act as host lattices) might be further favored by replacing phosphate groups by other related pseudotetrahedral anionic entities having a lower connectivity, such as occurs for hypophosphite groups.

The current knowledge on hypophosphites is scarce.[5] This is specially the case of transition metal derivatives. The only compounds whose structure has been determined are $Ni(H_2PO_2)_2 \cdot 6H_2O$,[6] β-$Mn(H_2PO_2)_2 \cdot H_2O$,[7] $Zn(H_2PO_2)_2 \cdot H_2O$,[7] $Zn(H_2PO_2)_2$,[7] $MCl(H_2PO_2) \cdot H_2O$ (M = Co, Ni),[8,9] α-$Mn(H_2PO_2)_2 \cdot H_2O$,[10] and $VO(H_2PO_2)_2 \cdot H_2O$.[11] In addition, three differently hydrated cobalt hypophosphites have been reported in the literature [$Co(H_2PO_2)_2 \cdot 6H_2O$,[6] $Co(H_2PO_2)_2 \cdot 2H_2O$,[13] and $Co(H_2PO_2)_2$[14]], but their structures remain unsolved. Our previous work on related systems[4] suggests that transition metal layered hypophosphites might be suitable host lattices to support intercalation reactions, although no successful attempt in this sense has been described in the literature to date.

Otherwise, solids with alternating inorganic and organic layers also have been extensively studied due to their useful sorptive and catalytic properties and because they can serve as microcrystalline models for interfacial systems.[15] Such compounds may formally be thought of as resulting from the intercalation of organic species into an inorganic host lattice.

In this work, we describe the synthesis and crystal structure of $Co(H_2PO_2)_2 \cdot nH_2O$ ($0 \leq n \leq 0.69$) solved from X-ray powder diffraction data. Moreover, we present for the first time a detailed study of intercalation processes into a transition metal hypophosphite host: the topotactic insertion of water and pyridine into $Co(H_2PO_2)_2$.

Experimental Section

Synthesis of $Co(H_2PO_2)_2 \cdot nH_2O$. An anhydrous variety of cobalt hypophosphite was reported by Brun and Dumail.[14] Unfortunately, the synthetic procedure was poorly described in their work (crystallization from aqueous solutions at 60 °C), and all our attempts to isolate it systematically lead to solids showing a variable degree of hydration. $Co(H_2PO_2)_2 \cdot 0.53H_2O$ was prepared as follows. A 2.851-g (10.1-mmol) sample of $Co(SO_4) \cdot 7H_2O$ were dissolved in 10 mL of distilled water.

* Abstract published in *Advance ACS Abstracts*, February 1, 1994.

(1) Whittingham, M. S.; Jacobson, A. J. *Intercalation Chemistry*; Whittingham, M. S., Jacobson, A. J., Eds.; Academic Press, New York, 1982.
(2) Murphy, D. W.; Sushine, S. A.; Zahurak, S. M. *Chemical Physics of Intercalation*; NATO ASI Series, Series B: Physics; Plenum: New York, 1987; Vol. 172, p 173.
(3) Clearfield, A. *Chem. Rev.* **1988**, *88*, 125.
(4) Beltrán, D.; Beltrán, A.; Amorós, P.; Ibáñez, R.; Martínez, E.; Le Bail, A.; Ferey, G.; Villeneuve, G. *Eur. J. Solid State Inorg. Chem.* **1991**, *28*, 131 and references therein.
(5) Loub, J.; Kratochvil, B. *Chem. Listy* **1987**, *81*, 337.
(6) Victor Chemical Works *Chem. Weekbl.* **1953**, *10*, 40.
(7) Weakley, T. J. R. *Acta Crystallogr., B* **1979**, *25*,42.
(8) Marcos, M. D.; Ibáñez, R.; Amorós, P.; Le Bail, A. *Acta Crystallogr., C* **1991**, *47*, 1152.
(9) Marcos, M. D.; Amorós, P.; Sapiña, F.; Beltrán, A.; Martínez-Mañez, R.; Attfield, J. P. *Inorg. Chem.* **1993**, *32*, 5044.
(10) Marcos, M. D.; Amorós, P.; Sapiña, F.; Beltrán, D. *J. Alloys Compd.* **1992**, *188*, 133.
(11) Le Bail, A.; Marcos, M. D.; Amorós, P. *Inorg. Chem.*, submitted for publication.
(12) Marcos, M. D.; Amorós, P.; Beltrán, A.; Beltrán, D. *Solid State Ionics* **1993**, *63–65*, 96.
(13) *Gmelin Handbook of Inorganic Chemistry*; Springer Verlag: Berlin, 1932; Vol. Co (58A).
(14) Brun, G.; Dumail, M. *C. R. Acad. Sci. Paris* **1971**, *272*, 1869.
(15) Cao, G.; Hong, H.; Mallouk, T. E. *Acc. Chem. Res.* **1992**, *25*, 420.

0020-1669/94/1333-1220$04.50/0

Over this solution, another one resulting from the neutralization (pH = 3) of 2.16 mL (20.2 mmol) of 30% H_3PO_2 with a saturated aqueous solution of $Ba(OH)_2$ was added while stirring. Precipitated $BaSO_4$ was eliminated by filtration. Then 75 mL of acetone were added over 30 mL of the resulting cobalt solution, and this mixture was heated to boiling (≈60 °C) during $^1/_2$ h. A pink-violet solid crystallized. It was separated by filtration, washed several times with a water/acetone mixture = 0.40 (volumetric ratio), and air dried. The X-ray diffraction pattern of the resulting solid was practically the same that Brun and Dumail attributed to anhydrous $Co(H_2PO_2)_2$.[14] Notwithstanding, a preliminary characterization of the product using IR spectroscopy revealed the presence of a certain amount of uncoordinated water in the solid. The water content was determined by thermogravimetric analysis, and the solid was consequently reformulated as $Co(H_2PO_2)_2{\cdot}0.53H_2O$ (Anal. Calcd for the anhydrous solid: Co, 31.2; P, 32.79. Calcd for the solid containing 0.53 water molecules/Co atom: Co, 29.72; P, 31.21. Found: Co, 29.74; P, 31.26.).

In a totally similar way, solids with different water content have been reproducibly obtained by varying the water/acetone ratio (R) in the final step. Anal. Calcd for R = 0.15, n = 0.05: Co, 31.05; P, 16.32; water, 0.47. Found: Co, 31.10; P, 16.29; water, 0.50. Calcd for R = 0.3, n = 0.22: Co, 30.56; P, 16.06; water, 2.05. Found: Co, 30.60; P, 15.98; water, 2.10. Calcd for R = 0.6, n = 0.69: Co, 29.28; P, 15.39; water, 6.17. Found: Co, 29.21; P, 15.47; water, 6.20. All these solids show nearly identical X-ray powder diffraction patterns, which are very similar to that obtained for the anhydrous Zn compound.[7] Under these conditions, higher R values do not lead to hypophosphite crystallization because of the deliquescence of the hypothetycal higher hydrated materials.

Synthesis of $Co(H_2PO_2)_2{\cdot}1.86(C_5H_5N){\cdot}0.31H_2O$. $Co(H_2PO_2)_2{\cdot}0.53H_2O$ (0.3 g; 0.88 mmol) was brought into contact with a solution containing 7 mL of acetone and 3 mL of pyridine (py). The mixture was maintained at room temperature during 10 h time with stirring. Then, the suspension was filtered, and the resulting pink solid was washed with acetone until all amine excess was removed. (Anal. Calcd: Co, 17.26; P, 9.07; water, 1.63; C, 32.68; N, 7.63; H, 2.72. Found: Co, 17.10; P, 9.21; water, 1.60; C, 32.60, N, 7.59; H, 2.69.)

Analysis. Cobalt and phosphorus contents were determined, after dissolution of the solids in boiling concentrated hydrochloric acid, by atomic absorption spectrometry (Perkin-Elmer Zeeman 5000). The amount of intercalated pyridine was determined by elemental analysis. Water was determined thermogravimetrically (Perkin-Elmer thermogravimetric analyzer TGA-7).

Physical Measurements. X-ray powder diffraction patterns were obtained from a Siemens D501 automated diffractometer using graphite-monochromated Cu Kα radiation. The diffractometer is equipped with a variable-temperature device working from room temperature to ca. 1000 °C. The pattern used for indexing was recorded with $Pb(NO_3)_2$ (analytical quality) as an internal standard, and scanned in steps of 0.02° in 2θ over the angular range 9–70° 2θ for 14 s per step. The TREOR program[16] was used to index the patterns. For Rietveld analysis, the pattern was collected with the same scanning step (0.02° in 2θ), but a wider 2θ range (5–125° in 2θ) and a longer acquisition time (20 s per step) to enhance statistics. In order to minimize preferred orientation effects, the sample holder described by McMurdie[17] was used. Rietveld profile analyses[18] were performed with the GSAS program[19] using a pseudo-Voigt peak shape function, corrected for asymmetry at low angles, and a refined background function. IR spectra (KBr pellets) were recorded on a FTIR Perkin-Elmer 1750 spectrophotometer. SEM observations were performed using a Hitachi 2500 microscope.

Results and Discussion

Synthesis and Characterization. We have recently described a synthetic approach intended to rationalize the solution preparative chemistry of transition metal phosphites and hypophosphites.[12] In that work, it was shown how, on the basis of simple ideas, it is possible to advance reasonable proposals concerning the main features of the metal environment in the resulting solids. For hypophosphites of divalent metal ions, the model predicts that, in moderately acid media, two water molecules would enter the metal coordination sphere. In practice, changes in the experimental conditions (*i.e.*, crystallization temperature, presence of non-aqueous solvents in the reaction media, etc.) may lead to solids in which the cationic environment contains one or no water molecules.[12,13] The elimination of coordinated water molecules from the metal environment requires the incoming of more oxygen atoms from $H_2PO_2^-$ anions. This implies, in turn, that these oxygen atoms would result in being shared by two metallic ions (*i.e.*, they would act as μ-O–hypophosphite bridges), giving rise to an enhancement of the cationic connectivity in the structure. This would be the case of the hypothetical anhydrous derivative, $Co(H_2PO_2)_2$,[14] which was suggested to be isostructural to the analogous zinc derivative $Zn(H_2PO_2)_2$.[7,14] For intermediate degrees of hydration ($0 < n < 2$), one might wonder whether water molecules belong or not to the coordination sphere of the cation.

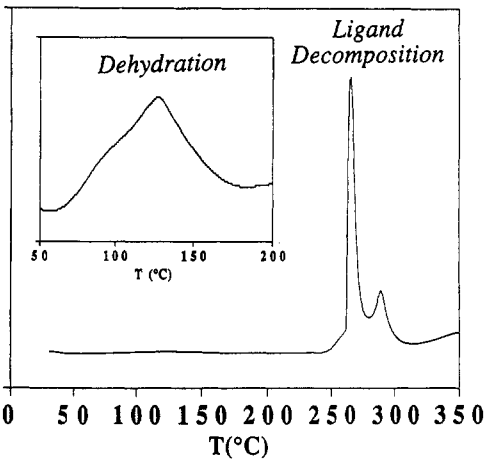

Figure 1. DSC plot for $Co(H_2PO_2)_2{\cdot}0.53H_2O$. Shown in the inset is the very small endothermic effect associated with water evolution.

In the case we are dealing with, $Co(H_2PO_2)_2{\cdot}nH_2O$ ($0 \le n \le 0.69$), all our experimental results support the idea that the water molecules present in the material must remain trapped in the interlamellar space. Thus, as mentioned above, all solids show XRD patterns very similar to that corresponding to the anhydrous $Zn(H_2PO_2)_2$.[7] On the other hand, TGA experiments show that, in all cases, water removal (whose associated weight loss begins to be observed at very low temperatures) is completed below 200 °C. Shown in Figure 1 is the DSC curve corresponding to $Co(H_2PO_2)_2{\cdot}0.53H_2O$. The very small endothermic effect (17.4 KJ·mol^{-1}) associated with water removal is indicative of very weak bonding interactions between the water molecules and the host lattice. Moreover the IR spectrum of $Co(H_2PO_2)_2{\cdot}0.53H_2O$ (Figure 2) shows, in addition to the bands characteristic of $H_2PO_2^-$ groups, broad bands centered at 3420, 3240, and 1630 cm^{-1} that can be assigned to the stretching and bending modes of uncoordinated water molecules.

On the other hand, as indicated in the Experimental Section, the water to acetone ratio in the reaction medium is the key variable (all the syntheses were carried out at a similar temperature, *ca.* 60 °C) controlling the final interlayer water molecule content. The presence of acetone in the medium, besides favoring water removal from the cobalt coordination sphere, may affect the crystallization rate of the resulting solid. In fact, a SEM study on these materials (whose lamellar morphology is clearly observed in all cases) has allowed us to establish a rather clear correlation between the final average particle size and the water content in the solids. Thus, whereas syntheses carried out at low acetone concentrations (*i.e.*, R = 0.60 for n = 0.69) lead to materials consisting of elongated platelets rather homogeneously sized (≈5 × 15 μm for n = 0.69), the presence of high acetone concentrations (*i.e.*, R = 0.15 for n = 0.05) results in small average particle size (≈1 × 5 μm, but unhomogeneous, for n = 0.05

(16) Werner, P. E. *Z. Kristallogr.* **1969**, *120*, 375.
(17) McMurdie, H. F.; Morris, M. C.; Evans, E. H.; Paretzin, B.; Wong, W.; Hubbard, C. R. *Powder Diffr.* **1986**, *1*, 40.
(18) Rietveld, H. M. *J. Appl. Crystallogr.* **1969**, *2*, 65.
(19) Larson, A. C.; Von Dreele, R. B. Los Alamos National Laboratory Rep. LA-UR-86-748, 1987.

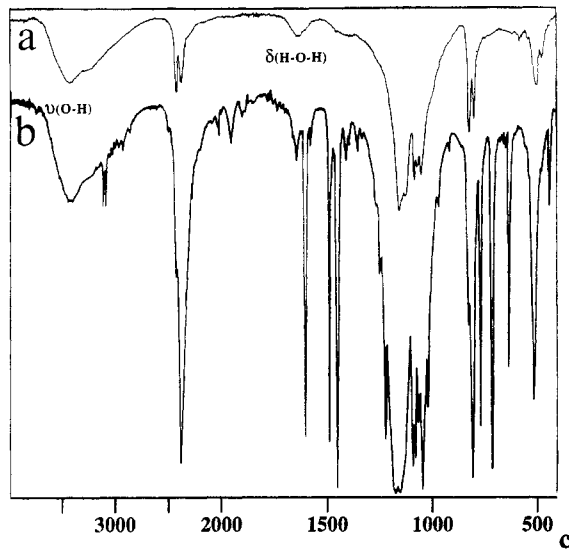

Figure 2. IR spectra (KBr pellet) of $Co(H_2PO_2)_2 \cdot 0.53H_2O$ (a) and $Co(H_2PO_2)_2 \cdot 1.86py \cdot 0.31H_2O$ (b). In part a, bands due to uncoordinated water molecules are located at 3420, 3240 cm^{-1} [υ(O–H)] and 1630 cm^{-1} [δ(H–O–H)]. Effects due to py intercalation are clearly seen in part b. Bands due to stretching C–H and ring vibrations are located around 3100 and 1500 cm^{-1}, respectively. Bending vibrations give bands around 1000 [δ(C–H)] and 500 cm^{-1} [δ(ring)].

materials). In short, as the acetone proportion in the reaction medium increases, the average particle size of the resulting solid gradually decreases (at the same time as the interlayer water content), which may be related to solubility factors retarding crystal growth. This relation between particle size and hydration degree should be consistent with the above mentioned poorly bonded ("zeolitic") nature of the water molecules: as in zeolites, water evolution should be a diffusion-controlled process along an intricate path from the inner to the grain boundary.

$Co(H_2PO_2)_2 \cdot 0.53H_2O$ Structure Refinement. The X-ray powder pattern of $Co(H_2PO_2)_2 \cdot 0.53H_2O$ was indexed from 21 accurately measured, unambiguous reflection positions. A primitive orthorhombic cell was obtained with the following parameters: $a = 7.478(2)$ Å, $b = 6.459(1)$ Å, and $c = 5.327(1)$ Å (figures of merit: $M_{20}=27$[20] and $F_{20}=21$ (0.012, 77)[21]). This cell was very close to that reported for $Zn(H_2PO_2)_2$,[7] despite its different water content. The systematic absences ($hk0$, $h = 2n + 1$; $h00$, $h = 2n + 1$) were consistent with the space group of the zinc compound, *Pmma*, among others. Therefore, the determination of the structure of the cobalt derivative was undertaken starting from the structural parameters of $Zn(H_2PO_2)_2$.[7] The refinement of the profile parameters and the atomic positions of the heaviest atoms easily converged giving rise to the accordance factors $R_{wp} = 29.5\%$ and $R_p = 21.2\%$. Notwithstanding, the positions of the oxygen atoms could not be refined. As the metallic ions were present in a very restrained position for the *Pmma* space group (2a position, $2/m$ symmetry), taking into account the nonregular octahedral coordination usually present for cobalt(II) ions, we tried the refinement in other space groups that allow a less symmetric metallic coordination. However, the other orthorhombic space groups that are compatible with the systematic absences, $Pmc2_1$ (Co ions in 2a position, m symmetry) and *Pma*2 (Co ions in 2a position, 2 symmetry), did not give better results. Only the monoclinic space group $P112/a$, in which the metallic ions lie in a 2a position with only -1 symmetry, starting from a value of the γ angle of 90.01°, allowed the refinement to be successfully carried out. The two lowest angle peaks of the diffractogram (001 and 010 reflections) were eliminated because of their large asymmetry. Anisotropic refinement of the thermal parameters for cobalt and phosphorus atoms was not possible. A Fourier difference map did not enable us to find either the water molecule, as expected, or the hydrogen atoms of the hypophosphite groups. The hydrogen positions were calculated considering the ideal C_{2v} geometries for $H_2PO_2^-$ anions. It was not possible to refine the position of the hydrogen atoms of the hypophosphite anions so they were fixed at their ideal values. The last refinement cycles were carried out with a soft constraint in the P–O bonds of the hypophosphite groups. The final reliability factors were $R_F = 5.4\%$, $R_p = 7.3\%$ and $R_{wp} = 9.0\%$. Details of the final refinement and atomic parameters are given in Table 1 and selected bond lengths and angles are listed in Table 2. Figure 3 shows the observed and calculated patterns.

(20) de Wolf, P. M. *J. Appl. Crystallogr.* **1968**, *1*, 108.
(21) Smith, G. S.; Synder, R. L. *J. Appl. Crystallogr.* **1979**, *12*, 60.

Table 1. Final Profile and Structural Parameters for $Co(H_2PO_2)_2 \cdot 0.53H_2O$ in the Space Group $P112/a$

Cell Constants

$a = 6.4722(3)$ Å	$V = 258.92(3)$ Å^3
$b = 5.3411(3)$ Å	$Z = 2$
$c = 7.4900(3)$ Å	no. of allowed reflcns: 830
$\gamma = 90.087(12)°$	no. of points in the refinements: 5500

Reliability Factors (%)[a]

$R_F = 5.38$	$R_p = 7.31$	$R_{wp} = 9.05$

Structural Parameters

atom	x/a	y/b	z/c	$100U_{iso}$,[b] Å^2
Co	0.0000	0.0000	0.0000	0.36(6)
P(1)	0.2500	0.5000	0.1478(5)	0.78(11)
P(2)	0.2500	0.0000	0.6277(5)	2.06(13)
O(1)	0.265(5)	0.2721(7)	0.0324(6)	1.7(2)
O(2)	0.0535(5)	0.003(6)	0.7352(6)	0.75(16)

[a] $R_F = 100\{\sum k[|F_k(\text{obsd})| - |F_k(\text{calcd})|]/\sum_k |F_k(\text{obsd})|\}$. $R_p = 100\{\sum_i |I_i(\text{obsd}) - I_i(\text{calcd})|/\sum_i |I_i(\text{obsd})|\}$. $R_{wp} = 100\{\sum_i \omega_i |I_i(\text{obsd}) - I_i(\text{calcd})|^2/\sum_i \omega_i |I_i(\text{obsd})|^2\}^{1/2}$. [b] U_{iso} = mean square displacement. $B_{iso} = 8\pi^2 U_{iso}$.

Table 2. Selected Interatomic Distances (Å) and Angles (deg) for $Co(H_2PO_2)_2 \cdot 0.53H_2O$[a]

Co Octahedron ⟨Co–O⟩ = 2.112

Co	O(2)	O(2)	O(1)	O(1)	O(1)	O(1)
O(2)	**2.013(4)**	4.03(4)	2.915(18)	2.93(2)	2.981(19)	3.07(2)
O(2)	180.0(2.1)	**2.013(4)**	2.93(2)	2.915(18)	3.07(2)	2.981(19)
O(1)	89.7(9)	90.3(9)	**2.119(14)**	4.24(2)	2.912(5)	3.27(3)
O(1)	90.3(9)	89.7(9)	180.0(1.0)	**2.119(14)**	3.27(3)	2.912(5)
O(1)	88.3(9)	91.7(9)	83.3(9)	96.7(1.2)	**2.259(14)**	4.52(2)
O(1)	91.7(9)	88.3(9)	96.7(1.2)	83.3(9)	180.0(1.0)	**2.259(14)**

P(1) Tetrahedron ⟨P–O⟩ = 1.348

P(1)	H(1)	H(1)	O(1)	O(1)
H(1)	**1.217(2)**	1.960(2)	2.253(9)	2.204(8)
H(1)	107.3(2)	**1.217(2)**	2.204(8)	2.253(9)
O(1)	111.8(5)	108.2(4)	**1.497(9)**	2.444(6)
O(1)	108.2(4)	111.8(5)	109.4(4)	**1.497(9)**

P(2) Tetrahedron ⟨P–O⟩ = 1.384

P(2)	H(2)	H(2)	O(2)	O(2)
H(2)	**1.210(2)**	1.960(2)	2.225(7)	2.189(8)
H(2)	18.2(2)	**1.210(2)**	2.189(8)	2.225(7)
O(2)	109.6(5)	107.0(5)	**1.505(7)**	2.544(4)
O(2)	107.0(5)	109.6(5)	115.3(7)	**1.505(7)**

Shortest Interlayer Distance and Selected Angles

O(2)···H(2)	2.941(19)	P(2)···O(2)	3.354(6)
	3.010(18)		3.354(5)
P(2)–O(2)–Co	132.2(1.1)	P(2)–O(2)···H(2)	100.9(4)
P(2)–H(2)···O(2)	99.2(3)	Co–O(2)···H(2)	124.3(6)
	95.7(4)		

[a] O(1) and O(2) positions: multiplicity 4; Wyckoff letter *g*; site symmetry 1; coordinates x, y, z; $-x + 1/2, -y, z$; $-x, -y, -z$; $x + 1/2, y, -z$.

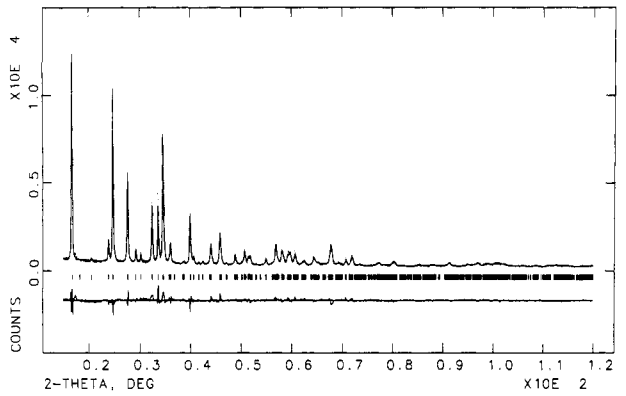

Figure 3. Observed and calculated X-ray diffraction patterns of $Co(H_2PO_2)_2 \cdot 0.53H_2O$. The difference pattern is at the same scale.

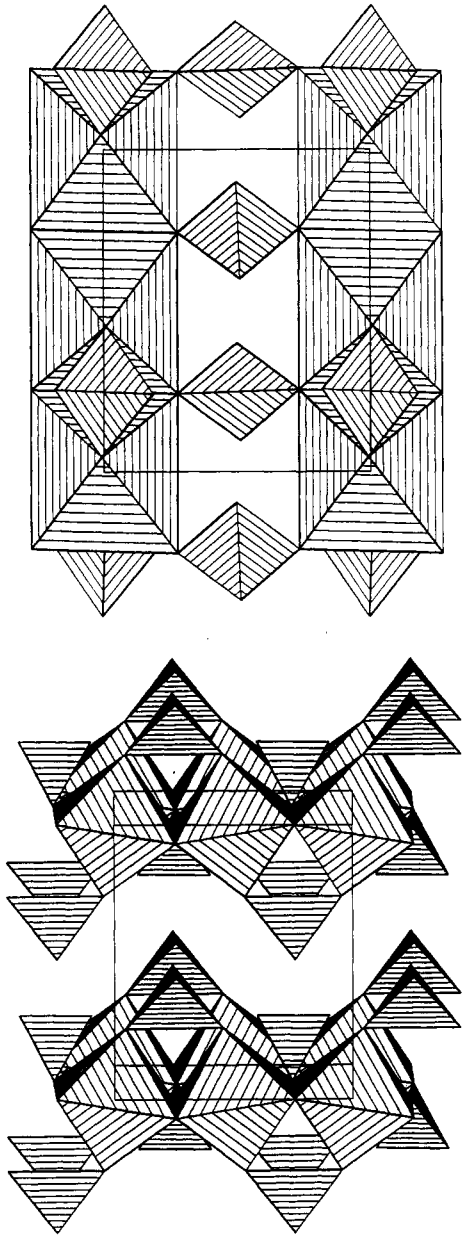

Figure 4. (a, top) Projection of the structure of $Co(H_2PO_2)_2 \cdot 0.53H_2O$ along the [001] direction showing the layer organization. (b, bottom) Perspective view along the [010] direction.

Description of the $Co(H_2PO_2)_2 \cdot 0.53H_2O$ Structure. Shown in Figure 4 are two projections of the $Co(H_2PO_2)_2 \cdot 0.53H_2O$ lamellar structure. The layers are identically constituted and electrically neutral, and apart from the water molecules, they should be connected through van der Waals bonds. The shortest distance between layers involves O(2) and H(2) atoms of P(2) hypophosphite groups (2.94(2) Å), which is longer than the sum of the intermolecular (van der Waals) standard radii (H, 1.17 Å; O, 1.52 Å).

Table 3. Bond Valence Analysis of $Co(H_2PO_2)_2 \cdot 0.53H_2O$ and $Zn(H_2PO_2)_2$

(a) $Co(H_2PO_2)_2 \cdot 0.53H_2O$

	Co		P(1)		P(2)		Σ
O(1)	0.24 (3) (x2)↓	→	1.41(3) (x2)↓	→			
	0.33(3) (x2)↓	→					1.98(9)
O(2)	0.43(3) (x2)↓	→			1.37(3) (x2)↓	→	1.80(6)
Σ	1.99(18)		2.82(6)		2.75(6)		

(b) $Zn(H_2PO_2)_2$

	Zn		P(1)		P(2)		Σ
O(1)	0.29(3) (x4)↓	(x2) →	1.39(3) (x2)↓	→			1.96(9)
O(2)	0.42(3) (x2)↓	→			1.43(3) (x2)↓	→	1.85(6)
Σ	1.99(18)		2.78(6)		2.85(6)		

The layers extend parallel to the *ab* plane and are built up from rutile type $[CoO_4]_n$ edge-sharing octahedra forming chains running along the [100] direction, joined together by means of hypophosphite bridges.

The metallic atom is found at the symmetry center surrounded by six oxygen atoms. As the octahedra share trans edges, the four oxygen atoms in the equatorial plane are each coordinated to two metallic centers, while the two apical oxygen atoms are only bound to one. This coordination mode gives rise to compressed metallic octahedra, with the axial Co-O distances being the shortest (Table 2).

There are two different hypophosphite groups in the structure. P(2) hypophosphites act as μ-(O,O′)-bridges, connecting each $[CoO_6]$ octahedron with its two neighbors in the chain through its apical positions. This bridging mode gives rise to tilting of the octahedra in such a way that an angle of 162.9(1)° between the equatorial planes of two adjacent octahedra results. Otherwise, P(1) hypophosphites are the responsible for the interchain connections (μ-(O,O′) bridges) building up the layers. Moreover, in each chain, P(1) hypophosphites act as μ-(O) bridges, occupying the shared oxygen atom an equatorial position in the $[CoO_6]$ octahedra. In this way, connections of the type $\cdots(M^I, M^I)$–O^I–P(1)–O^{II}–(M^{II}, M^{II})–O^{II}–P(1)–O^{III}–$(M^{III}, M^{III})\cdots$ (different superindices indicate different [100] chains) are established along the [010] direction.

The bond valence analyses[22] of $Co(H_2PO_2)_2 \cdot 53H_2O$ and $Zn(H_2PO_2)_2$ (from data in ref 7) are gathered in Table 3, both showing very close values. The cationic valence is in good accordance with the expected value of two (1.99(18) valence units for both cations, cobalt and zinc) and the O(1) atoms also show a quite saturated valence. The bond valences for the phosphorus atoms are low, presumably due to the P–H bonds that have not been taken into account in the calculations. However, it is important to note that O(2) atoms also have low bond valences (1.80(6) and 1.85(6) valence units for the cobalt and zinc compounds, respectively). Though the position of the water molecules has not been found in the refinement, taking into account this deficient valence and the position of these O(2) atoms, it seems reasonable to think about the formation of hydrogen bonds involving O(2) atoms and water molecules.

Shown in Figure 5 is the variation of the cell parameter values vs n for $Co(H_2PO_2)_2 \cdot nH_2O$ samples (values corresponding to

(22) Brese, N. E.; O'Keeffe, M. *Acta Crystallogr., B* **1991**, *47*, 192.

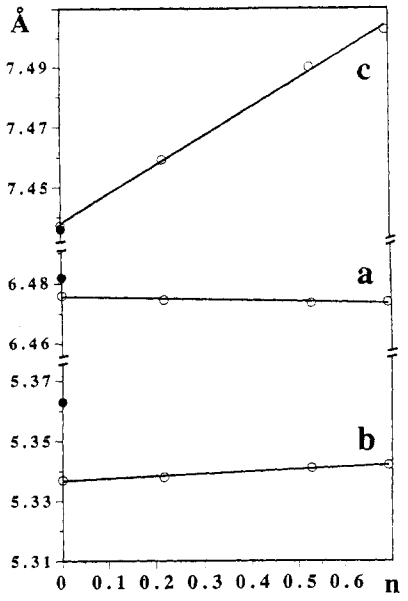

Figure 5. Variation of the cell parameters *vs* n for $Co(H_2PO_2)_2 \cdot nH_2O$ (○). Cell parameters of the Zn anhydrous derivative, $Zn(H_2PO_2)_2$ (●), are included for comparison.

$Zn(H_2PO_2)_2$ are included for comparison). Dealing with the cobalt derivatives, the a, b, and γ parameters remain practically unchanged, but there is a gradual increase in the c parameter when the water content increases. On the other hand, the main difference between the anhydrous zinc and cobalt compounds concerns the layer (*i.e.*, a and b) parameters. All these tendencies can clearly be related to the fact that the in-plane parameters (a, b, and γ) are governed by the cationic packing. They consequently vary in the same sense as the ionic radii. Conversely, the c parameter is governed by the layer separation and, therefore, it is less sensitive to ionic radii variations, being much more sensitive to the presence of guest molecules in the interlayer space.

Water Intercalation. To investigate the reversibility of the water insertion process in the host lattice, we approached the study of the dehydration/rehydration reaction by means of thermal analysis and X-ray powder diffraction techniques. This study has been carried out on samples of three differently hydrated $Co(H_2PO_2)_2 \cdot nH_2O$ solids: n = 0.22, 0.53, and 0.69. Thermogravimetric multiramp experiments have been performed using the same temperature profile and conditions for all of the samples. The temperature profile is defined by four consecutive steps: (1) 3° min^{-1} heating ramp, (2) 30 min dwell at 180 °C, (3) −3° min^{-1} cooling ramp, and (4) 600 min dwell at 25 °C. The two last steps have been carried out under an H_2O-saturated argon flowing atmosphere in order to rehydrate the samples. The thermal evolution of the samples is represented in Figure 6 and is qualitatively similar for all of them.

Dehydration begins at room temperature, and the temperature range along which the process is completed increases with the sample water content (dehydration is completed at 80, 140, and 175 °C for solids containing 0.22, 0.53, and 0.69 water molecules per metal atom, respectively). When cooling, the rehydration process begins at the same temperature (50–60 °C) for all three solids, and the sample weight increases rapidly at room temperature. Whereas in no case complete rehydration occurs, both the rehydration rate and the rehydration degree are higher for smaller n values.

On the other hand, we have approached the study of the formal kinetics of the dehydration process using thermogravimetric data. The values of the kinetic parameters have been estimated firstly from the mathematical approach of Abou-Shaaban and Simonelli.[23] Then, these parameters have been used as reference criteria for elucidation of the formal mechanism by nonisothermal procedures (applied to the same data set), using the Satava integral method[24] to analyze the more widely assumed models for the kinetic study of solid state reactions.[25] To shorten, only values provided by the models leading to the best fit have been included in Table 4.

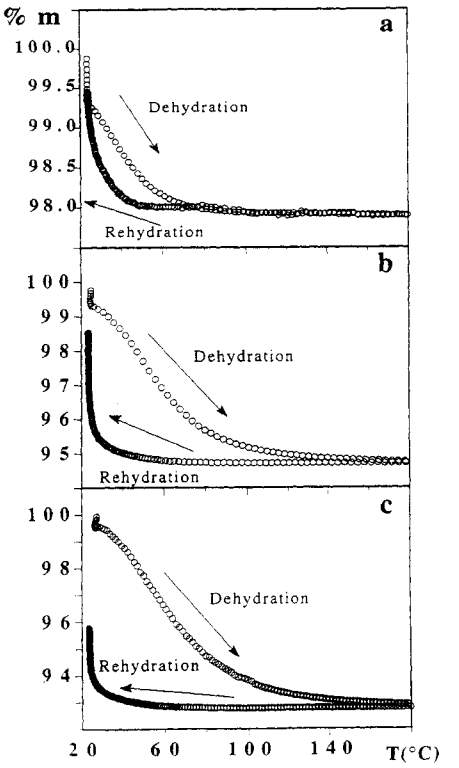

Figure 6. Thermal evolution of $Co(H_2PO_2)_2 \cdot nH_2O$ (n = 0.22, 0.53, 0.69) showing the dehydration and rehydration processes. (a) n = 0.22; (b) n = 0.53; and (c) n = 0.69.

Table 4. Kinetic Parameters

	Abou-Shaaban		Satava		
n	ΔH^*, kJ/mol	Z	ΔH^*, kJ/mol	Z	model[a]
0.22	12.3	10^2	13.8	10^2	A_2
0.53	20.3	10^2	21.6	10^3	D_2
0.69	25.9	10^2	25.2	10^2	D_2

[a] Sharp's notation.[26]

From our analysis, two different dehydration patterns are possible: (a) in the case of $Co(H_2PO_2)_2 \cdot 0.22H_2O$, the rate-controlling step in the water evolution process follows a random nucleation model (A_2); (b) $Co(H_2PO_2)_2 \cdot nH_2O$ solids with n = 0.53 and 0.69, behave similarly and water elimination obeys a diffusion-controlled mechanism (D_2). From these data, the following statements could be made: (a) in the case of the less hydrated solid (n = 0.22), the diffusion process should not be severely hindered probably because of the low particle size; (b) on the contrary, when the particle size increases, n = 0.53 and 0.69, water elimination is diffusion controlled and the activation enthalpy increases slightly; (c) in all cases, the low activation enthalpy values are consistent with very weak interactions between hypophosphite layers and water molecules.

Additionally, the formal kinetics of the rehydration processes of all three solids (n = 0.22, 0.53, 0.69) was studied. After the

(23) Abou-Shaaban, R. R. A.; Simonelli, P. *Thermochim. Acta* **1978**, *26*, 67; **1978**, *26*, 89.
(24) Satava, V. *Thermochim Acta* **1971**, *2*, 423.
(25) Hulbert, S. F. *J. Br. Ceram. Soc.* **1979**, *8*, 11.
(26) Sharp, J. H.; Brindley, G. W.; Achar, N. N. *J. Am. Ceram. Soc.* **1966**, *47*, 379.

anhydrous solids were cooled, isothermal experiments were performed at 25 °C under a humidified N_2 atmosphere. When $\ln[-\ln(1-x)]$ is plotted as a function of $\ln(t)$, a comparison with the theoretical slopes characteristic of the different models allow us to determine the more probable reaction mechanism. In all three cases, a three-dimensional phase boundary model (R_3) can be inferred for the rehydration process. Accordingly, the more hindered step in the rehydration process seems to be the layer rearrangement.

In any case, as mentioned above, rehydration does not go to completion. The fact that it progress faster and further on (see Figure 6) in the case of the initially lower hydrates might be related to their small particle size allowing shorter paths from the surface to the inside of the grains.

Otherwise, the X-ray powder diffraction patterns of all three hydrates are very similar and are also similar to those recorded at different temperatures in the course of their respective dehydration processes. Calculated lattice constants are in good agreement with those observations reflected in Figure 5. Results from time and temperature resolved X-ray powder diffraction experiments on $Co(H_2PO_2)_2{\cdot}0.53H_2O$ show that the crystal structure of the host lattice is preserved during the dehydration reaction until 240 °C. Then, ligand degradation occurs, leading to an amorphous solid. The IR spectrum of the decomposition product shows the presence of HPO_3^{2-} entities, which is in accordance with the well known disproportionation of hypophosphite into phosphite and phosphine.[27]

Pyridine Intercalation. $Co(H_2PO_2)_2{\cdot}nH_2O$ compounds react with pyridine to give crystalline intercalation products having, approximately, two inserted pyridine molecules. The simplest preparation procedure is to put into contact (acetone suspension) the hypophosphite host lattice and pyridine with continuous stirring for some time. It must be noted that intercalation only occurs, however, when the pyridine to acetone ratio in the medium reachs a threshold value (py to acetone molar ratio equal to 0.4). Lower pyridine proportions do not yield intercalates and, on the other hand, in the presence of high pyridine amounts (py/acetone > 0.5) amorphous products result. Pyridine intercalation does not modify significantly (as shown by UV–vis spectroscopy) the pale pink color of the matrix, $Co(H_2PO_2)_2$, this suggesting that the cobalt environment is not noticeably altered in the process.

Infrared spectroscopy can be used to distinguish various modes of pyridine binding in solids. Studies on alumina surfaces have allowed workers to distinguish among physisorbed pyridine, Brönsted-coordinated pyridine, and Lewis-coordinated pyridine.[28] The infrared spectrum of $Co(H_2PO_2)_2{\cdot}1.86py{\cdot}0.31H_2O$ is shown in Figure 2. The strongest IR band characteristic of Brönsted-bound pyridine, *i.e.* pyridinium ion, which should appear at 1540 cm^{-1}, is not present in this spectrum (Figure 2). Both the position and the relative intensities of all bands due to pyridine vibrations are very close to that reported for pure pyridine samples or non-coordinated pyridine containing solids.[29]

Figure 7 shows the TGA curve for $Co(H_2PO_2)_2{\cdot}1.86py{\cdot}0.31H_2O$. Three steps can be distinguished in the course of its decomposition. The first one corresponds to the dehydration process, the second one to pyridine evolution, and the last one to hypophosphite disproportionation. As in the case of $Co(H_2PO_2)_2{\cdot}nH_2O$, water evolution begins at very low temperature. Pyridine deintercalation occurs in the temperature range from 75 to 145 °C. The low-temperature values at which pyridine is removed from the host matrix, which are very similar to the pyridine boiling point, reveal that this organic molecule interacts

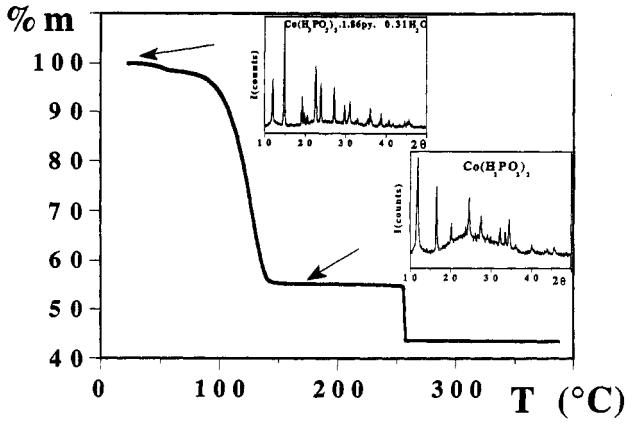

Figure 7. TGA curve for $Co(H_2PO_2)_2{\cdot}1.86py{\cdot}0.31H_2O$ showing the reversible character of the py intercalation reaction. Shown in the insets are the X-ray powder diffraction patterns of $Co(H_2PO_2)_2{\cdot}1.86py{\cdot}0.31H_2O$ and $Co(H_2PO_2)_2$, respectively.

weakly with the cobalt hypophosphite layers. This fact, which is in good agreement with the IR data, confirms that pyridine molecules are not coordinated to the metal cations. Actually, thermal data on vanadium and niobium phosphates containing amines show that significantly higher temperatures (ranging from 500 to 600 °C) are needed in order to eliminate Brönsted or Lewis bounded amines.[30-32]

Formal kinetics of the deintercalation process has been studied by the same procedures mentioned above. In the case of $Co(H_2PO_2)_2{\cdot}1.86py{\cdot}0.31H_2O$, and concerning the pyridine evolution step, the Z and ΔH values calculated using the Abou-Shaaban method ($Z = 10^5$, $\Delta H = 94.1$ kJ·mol^{-1}) are in rather good agreement with those found by the Satava procedure ($Z = 10^6$, $\Delta H = 104.5$ kJ·mol^{-1}) when a D_2 model is assumed. Thus, as for water evolution in $Co(H_2PO_2)_2{\cdot}nH_2O$ ($n = 0.53, 0.69$), the pyridine evolution rate seems to be controlled by a diffusion mechanism.

An interesting aspect of this process is the reversible character of the pyridine insertion reaction. So, the plateau observed between 140 and 250 °C in the TGA curve in Figure 7 can be associated (weight loss and XRD pattern) with the formation of $Co(H_2PO_2)_2$. Actually, apart from the low crystallinity of the solid, the main features of the X-ray powder diffraction pattern of a pyridine-containing sample, $Co(H_2PO_2)_2{\cdot}1.86py{\cdot}0.31H_2O$, after heating at 200 °C for 30 min (see inset in Figure 7), are coincident with those observed in the pattern of $Co(H_2PO_2)_2$.

The X-ray powder diffraction pattern of $Co(H_2PO_2)_2{\cdot}1.86py{\cdot}0.31H_2O$ can be indexed on a triclinic cell of dimensions $a = 5.623(3)$ Å, $b = 6.782(3)$ Å, $c = 16.471(6)$ Å, $\alpha = 67.03(3)°$, $\beta = 91.92(4)°$, $\gamma = 77.31(4)°$ (see Table 5). Other triclinic solutions are possible, and our choice is based not only on the good agreement between the observed and calculated d values but also on constraining the layer dimensions to be as close to those of the anhydrous compound as possible. Pyridine intercalation should not disturb appreciably the layer bonding scheme, and it only should modify the interlayer distance, which expands from 7.4 to 16.47 Å ($\Delta d = 7.70$ Å).

On the basis of the calculated cell parameters, a tentative explanation about the effect of the intercalated pyridine might be advanced. The a parameter value (5.623 Å) is close to that observed in $Co(H_2PO_2)_2{\cdot}0.53H_2O$. Hence, a similar μ-(O,O′)-H_2PO_2 bridging scheme among the rutile type chains stacked at the same c level might be formed. Otherwise, the b cell parameter

(27) Baran, E. J.; Etchevarry, S. B.; Diemann, E. *Polyhedron* **1985**, *4*,1711.
(28) Matulewicz, E. R. A.; Kerkhof, F. P. J. M.; Moulijn, J. A.; Reitsma, H. J. J. *Colloid Interface Sci.* **1980**, *77*, 110. Perry, E. P. *J. Catal.* **1963**, *2*, 371.
(29) Silverstein, R. M.; Bassler, G. C.; Morrill, T. C. *Spectrometric Identification of Organic Compounds*; John Wiley & Sons, Inc.: New York, 1963.
(30) Johnson, J. W.; Jacobson, A. J.; Brody, J. F.; Rich, S. M. *Inorg. Chem.* **1982**, *21*, 3820.
(31) García-Ponce, A. L.; Moreno-Real, L.; Jimenez-López, A. *J. Solid State Chem.* **1990**, *87*, 20
(32) Savariault, J. M.; Lafarge, D.; Parize, J. L.; Galy, J. *J. Solid State Chem.* **1992**, *97*, 169.

Table 5. X-ray Powder Diffraction Data for $Co(H_2PO_2)_2 \cdot 1.85py \cdot 0.31H_2O$ (λ = 1.5418 Å)

$2\theta_{obsd}$, deg	d_{obsd}, Å	d_{calcd}, Å	*h k l*	I/I_0, %
11.782	7.511	7.514	0 0 2	47
14.664	6.041	6.041	0 1 0	100
16.300	5.438	5.438	1 0 0	9
19.001	4.671	4.671	1 1 0	33
20.264	4.382	4.383	1 1 2	14
21.392	4.154	4.151	1 0 2	13
23.695	3.754	3.757	0 0 4	43
27.004	3.302	3.303	-1 0 4	44
29.550	3.023	3.020	0 2 0	27
30.848	2.899	2.901	1 -1 2	30
32.734	2.736	2.731	0 -1 4	14
34.691	2.586	2.586	-1 2 2	10
35.262	2.545	2.543	-2 -1 2	14
35.861	2.504	2.505	0 0 6	21
37.976	2.369	2.370	2 2 2	19
41.464	2.178	2.180	0 3 2	10
44.377	2.041	2.043	-1 -1 6	11
45.018	2.014	2.014	0 3 0	10
45.463	1.995	1.994	1 3 6	5
48.484	1.878	1.877	-1 3 2	7
50.181	1.818	1.818	-3 0 2	11
53.665	1.708	1.707	1 0 8	10
56.338	1.633	1.633	-1 -1 8	9
58.997	1.566	1.565	1 2 10	7
62.899	1.478	1.477	-1 4 6	10
64.220	1.450	1.451	2 -2 4	9
68.117	1.377	1.377	2 3 10	9

expands slightly from $Co(H_2PO_2)_2 \cdot 0.53H_2O$ to the solid containing pyridine. This effect might be associated to a less corrugated character of the rutile-type chains. So, it seems reasonable to assume that the intralayer bonding scheme is maintained in the pyridine containing solid and that the increase observed in the γ angle only implies a relatively small displacement of the rutile-type chains. Finally, the increase of the *c* parameter value due to pyridine insertion, despite its seemingly high value (resulting in Δd = 7.70 Å), is relatively small when compared to the induced effect in other lamellar materials such as $VOPO_4$ (for which Δd = 5.15 Å).[30] At this point, it must be remarked that the pyridine to metal ratio in the intercalate is close to 2 in the cobalt material, whereas only one pyridine molecule per metal atom enters the vanadium material. In the latter, each pyridine molecule coordinates one vanadium atom, giving rise to a bonding scheme in which the intercalated molecules stand perpendicular to the layers.[30] The unlikelihhod of such an arrangement in $Co(H_2PO_2)_2 \cdot 1.86py \cdot 0.31H_2O$ is suggested by the weakly bonded character of pyridine and the relatively small expansion detected by X-ray diffraction, as well as by the observation that all IR bands due to pyridine vibrations are not dichroic. This last result also allows us to discard an arrangement of the pyridine molecules parallel to the *ab* plane. So, although more work is needed to elucidate unambiguously this point, it might tentatively be proposed a two by two stacking mode of the pyridine molecules following the corrugated layout of the interlamellar space. Taking into account the van der Waals pyridine out of plane diameter (3.4 Å), such an arrangement, which would require a void of $6.8/(\cos\theta)$ Å (θ being the angle defined by the pyridine axis and the *c* direction), might explain the experimental increase of the interlayer distance, Δd = 7.70 Å.

Concluding Remarks

The intercalation reactions described in this work constitute the first examples in which a layered transition metal hypophosphite acts as host lattice. The low connectivity of pseudotetrahedral species such as hypophosphite and related anions results in the formation of a variety of bidimensional systems. It seems that intercalation chemistry can rapidly widen its scope by exploring both other related possible host lattices (such as, for example, $MCl(H_2PO_2) \cdot H_2O$ ($M = Co^{2+}, Ni^{2+}$),[8,9] $M(HPO_3) \cdot H_2O$ ($M = Co^{2+}, Ni^{2+}$)[9,33]) and a great diversity of guest species. The latter would allow, in turn, to progress further on in the alluring field of alternating inorganic–organic layered solids.

Acknowledgment. We thank the Institució Valènciana dEstudis i Investigació (IVEI) and the DGI.CYT of the Spanish Ministerio de Educación y Ciencia (PB91–0495) for financial support of this work. M.D.M. thanks the Spanish Ministerio de Educación y Ciencia for a FPI fellowship. The SCME of the University of Valencia (Spain) is acknowledged for the SEM facilities.

(33) Sapiña, F.; Gómez-Romero, P.; Marcos, M. D.; Amorós, P.; Ináñez, R.; Beltrán, D.; Navarro, R.; Rillo, C.; Lera, F. *Eur. J. Solid State Inorg. Chem.* **1989**, *26*, 603.